EXPERIMENTAL INVESTIGATION INTO THE VORTEX RING STATE OF MULTI-ROTOR CONFIGURATIONS

D.J. Pickles, D. Zagaglia*, A.D. Croke, R.B Green
James Watt School of Engineering, University of Glasgow
University Avenue, Glasgow, G12 8QQ, Scotland, UK
* Corresponding Author, e–mail: daniele.zagaglia@glasgow.ac.uk

Abstract

This paper presents an experimental investigation of the effect of rotor separation on the structure of the flow field produced by a quadcopter operating in axial descent by means of Particle Image Velocimetry (PIV). PIV was used to investigate the flow for a range of quadcopter rotor configurations and descent velocity ratios and results were compared with those produced by a tandem rotor. Time-averaged data was used to characterise the general structure of the flow field, whilst the unsteady features of the flow were investigated using a statistical analysis of the velocity fluctuations. It was found that for low enough rotor spacings, the wakes of the four rotors coalesce as a single wake. In this case, when the descent velocity is increased, the quadrotor undergoes one single, global, vortex ring state instead of four separate ones, one per rotor.

Keywords: Quadcopter, Vortex Ring State, Particle Image Velocimetry, Wind Tunnel.

NOMENCLATURE

Symbols

A_D	Rotor disc area, (m^2)
c	Rotor Mean Chord, (m)
D	Rotor diameter, (m)
M	Magnification factor, ($pixel/mm$)
R	Rotor radius, (m)
Re	Reynolds number, ($-$)
S	Hub to hub distance, (m)
U_i	Notional induced velocity, (m/s)
U_o	Free stream velocity, (m/s)
V_t	Rotor blade tip velocity, (m/s)
(u, v, w)	Velocity components, (m/s)
(x, y, z)	Cartesian coordinate system, ($-$)
α	Descent ratio, U_i/U_o ($-$)
Δt	Laser pulse Time delay, (μs)
σ	Solidity, $Nc/\pi R$, ($-$)
Ω	Rotational frequency, (RPM)

Acrynoms

CMOS	Complementary Metal Oxide Semiconductor
eVTOL	Electric Vertical Take-off and Landing
PIV	Particle Image Velocimetry
RMS	Root Mean Square
ROI	Region of Interest
RPM	Revolutions Per Minute
UAV	Unmanned Aerial Vehicle
VRS	Vortex Ring State

1. INTRODUCTION

The Vortex Ring State (VRS) is a dangerous flight condition that can occur when helicopters (Ref. [1]), tandem rotors (Ref. [2]), tiltrotors (Ref. [3, 4, 5]), and multi-rotor unmanned aerial vehicles (UAVs) descend into their own wake. For isolated rotors operating in axial descent, when the descent velocity approaches the hover induced velocity of the rotor, the system of intertwined helical vortices that trail from the rotor blades collapse, forming a highly unsteady vortex ring of a similar scale to that of the rotors diameter (Ref. [6]). Aperiodic shedding of the vortex ring usually leads to: a reduction in the mean thrust of the rotor, an increase in the average power required, large and mostly aperiodic oscillations in the rotor loading leading to yaw and roll oscillations, and eventually the loss of control efficiency which can potentially lead to the loss of the aircraft, as shown in Ref. [7, 8]. For tiltrotors the VRS can also cause "roll-off" which occurs because of thrust asymmetry that can occur between the two rotors (Ref. [3, 5, 9, 10]).

Early investigations performed by Washizu et al. (Ref. [3]), Betzina (Ref. [4]) and Abrego et al. (Ref. [5]), showed that for counter-rotating (side by side) propellers, the presence of the second rotor increased the size of the flight envelope in which the VRS occurred when compared to an isolated rotor. Experiments by Abrego et al. into the flow field produced by a pair of rotors arranged in close proximity, Ref. [5], indicated that the simulated image plane used by Washizu et al. to simulate the VRS of side by side rotors did not fully replicate the interference effects between the two rotors. However, the presence of a second rotor was found to alter the response of the rotors helical shed vortices, increasing the growth rate of disturbances to the vortex system, therefore making them more susceptible to breaking down into the torus associated with the VRS.

An experimental investigation by Chae et al. into the effect rotor separation has on the development of the wake produced by tandem rotors, Ref. [11], showed that rotor-rotor interactions can significantly affect the structure of the wake produced when they are operating in axial descent. In hover, at rotor separation distances (tip-tip) less than one radius, the wake from the two rotors merge together, rather than propagate away from the rotor disc plane independent of each other. In axial descent, at large rotor spacings, the rotors behaved like isolated rotors, forming individual VRSs. However, at smaller spacings asymmetric formations of the VRS, resulting from the interaction of the large regions of recirculating air generated, were observed. At smaller rotor separations of a quarter radius, it was shown that a global VRS forms as a result of the rotor-rotor interactions.

The majority of the research into multi rotor systems, such as UAVs and electric vertical take off and landing (eVTOL) aircraft, has focused on their control or on characterising and subsequently optimising the thrust produced by the vehicle operating in both hover and forward flight. This was achieved through the optimisation of blade design, spacing or phasing. With respect to descent flight, UAV pilots are taught to avoid the VRS by carefully controlling the rate of axial descent and avoiding areas susceptible to large up drafts of air. If the drone enters the VRS, the application of full throttle is often insufficient to prevent the drone descending and alternative manoeuvres must be implemented to prevent the drone from crashing, similarly to the Vuichard recovery technique.

Research into the structure of the flow field produced by these vehicles in descent flight has been extremely limited despite the dangers associated with the VRS, as these configurations have been shown by Brown, Ref. [12], to be more susceptible to VRS than standard rotorcraft under certain design conditions. With this in mind, given the large number of UAVs and multi-rotor eVTOL aircraft that are currently in development, it seems prudent that a more thorough understanding of the effect different rotor configurations have on the development and manifestation characteristics of the VRS is required to ensure the safety of these aircraft.

This paper presents an experimental investigation designed to investigate the effect of rotor separation on the structure of the flow field produced by a quadcopter operating in axial descent by means of Particle Image Velocimetry (PIV). PIV was used to investigate the flow for a range of quadcopter rotor configurations and descent velocity ratios and results were compared with those produced by a tandem rotor. Time-averaged data was used to characterise the general structure of the flow field, whilst the unsteady features of the flow were investigated using a statistical analysis of the velocity fluctuations.

2. EXPERIMENTAL SETUP

2.1. Rotor Test Rig

For this investigation a custom quadcopter test rig, which allowed the rotor separation (hub to hub distance) (S) to be varied from $6R$ to $3R$ with $1R$ increments was manufactured. Four $0.127m$ diameter (D), 3 bladed, fixed pitch $5030DTI$ propellers with a characteristic chord length of $c = 0.015m$ and a solidity of $\sigma = 0.226$ were mounted onto four Ultra 2806 (2206 Stator): $2300KV$ brushless motors. The rotors had no cyclic, and there was no lead lag or flap degrees of freedom. Each of the propellers was operated at a constant rotational frequency $\Omega = 30Hz$ $(1800RPM)$, thereby producing a blade tip velocity $V_t = 12\ m/s$ and rotor tip Reynolds number of $Re = 12,600$. A schematic diagram of the test rig installed in the wind tunnel is shown in Fig. 1. The quadcopter was configured in a standard "+" configurations with two rotors rotating in the clockwise direction and two rotors spinning counterclockwise. All the rotors lay in the same plane. A schematic diagram of the displacements of the rotors and the respective rotational directions is shown in Fig. 2. In order to investigate the effect the two out-of-plane rotors had on the structure of the flow field, the experiments were repeated with the two lateral rotors (dashed lines in Fig. 2) turned off, henceforth know as the tandem rotor configuration.

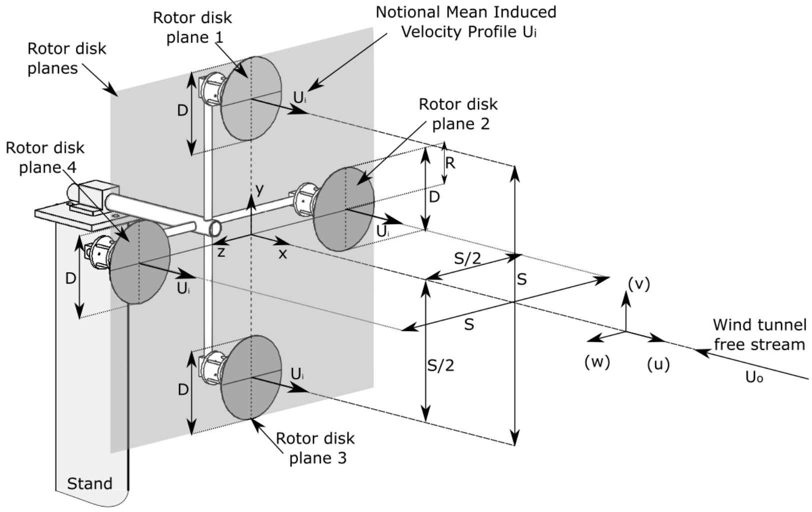

Figure 1: Schematic diagram of the quadcopter test rig installed in the Handley Page wind tunnel. Adopted reference system is shown also.

The rotors were orientated to induce velocity U_i against the wind tunnel free stream U_o, thereby simulating axial descent. The counterflow was generated using the University of Glasgow, Handley Page low-speed, closed return wind tunnel which is capable of achieving wind speeds of up to $50m/s$ in the $2.1m$ wide by $1.5m$ high octagonal test section. The quadcopter test rig was exposed to a range of descent velocity ratios ranging from $\alpha = U_i/U_o = 0$ to 2. The test rig shown in Fig. 1 had a negligible wind tunnel blockage of approximately 2% based on the four rotor disc areas.

An (x,y,z)-cartesian coordinate system with its origin at the geometric centre of the test rig was defined such that the x-axis is in the plane of the wind tunnel free stream and the y-axis is orientated vertically upwards as shown in Fig. 1.

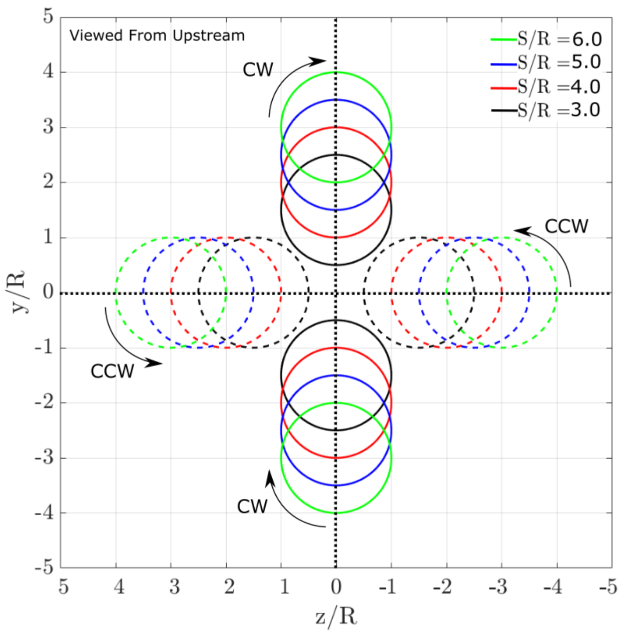

Figure 2: Schematic diagram showing the different rotor spacings and rotational directions investigated in both quadcopter and tandem rotor configurations, seen from upstream. In tandem configuration, the two lateral rotors (dashed lines) were not operated.

2.2. PIV Setup

A 2 component Particle Image Velocimetry (PIV) of a plane spanning the $x-y$ plane was used to investigate the structure of the flow field produced. A schematic diagram showing the region of interest (ROI) investigated is shown in Fig. 3, together with a sub-ROI utilised for the visual representation of the flow in some figures of section 3.2. A 532nm wavelength Litron Bernoulli 200-15 PIV laser with an energy output of 200mJ per pulse was used to produce the light sheet. A LaVision Imager CX-16 camera with a 5312 x 3024 pixel CMOS sensor fitted with a Nikon Nikkor 50 mm lens ($f/1.2$) was used to acquire the raw images. Homogeneous seeding of the wind tunnel was achieved using a Pea Soup PS27 Dragon smoke generator installed at the outlet of the test section, with a maximum oil particle diameter of $0.3\mu m$. 500 image pairs were recorded at a frequency of 14 Hz with a time delay of $\Delta t = 150\mu s$ for all experimental configurations investigated.

Post processing of the raw PIV images was completed using DAVIS V10.2. Laser glare on the pro-

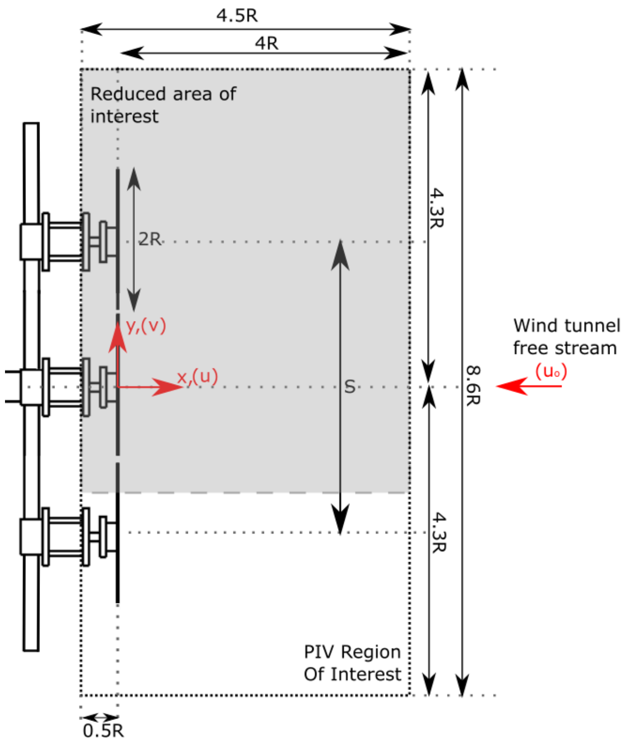

Figure 3: Schematic diagram of the full and reduced PIV regions of interest for the quadcopter and tandem rotor operating in axial descent.

peller spinner prevented reliable data from being acquired within 4 mm of the propeller hub. In some configurations the presence of the two lateral propellers could be observed in the ROI as a consequence of perspective, therefore in some configurations a mask was applied to remove this from the data analysis.

The PIV velocity fields were produced using a multi-pass cross correlation algorithm with interrogation windows of 64 x 64 pixels with a 50% overlap, followed by an interrogation window of 32 x 32 pixels with a 50% overlap. The resolution was 0.026R (approximately 80 velocity vectors over the rotor diameter) and had a magnification factor $M = 9.53$ pixels/mm. Assuming a maximum displacement error of 0.1 pixels owing to a sub-pixel interpolation, the uncertainty of the PIV velocity measurements was therefore estimated using Ref. [13] to be approximately, $0.1/(M\Delta t) = 0.07\ m/s$.

Flow field statistics were then computed and the unsteadiness of the flow field was assessed by calculating the root mean square (RMS) of the fluctuations of the instantaneous axial velocity from the mean axial velocity.

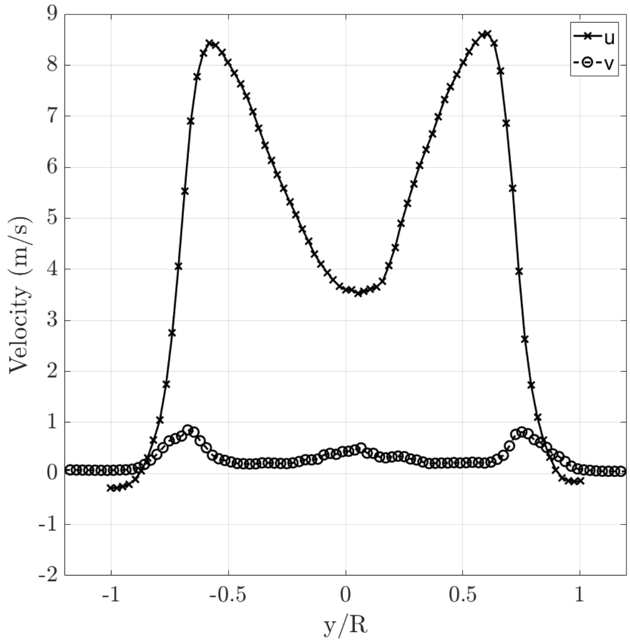

Figure 4: Axial velocity component of the isolated rotor, operating in hover, on a plane $x/R = 0.48$ from the rotor disc plane.

3. RESULTS AND DISCUSSION

3.1. Flow Field Characterisation In Hover

3.1.1. Isolated Rotor

The flow field produced by an isolated rotor in hover was initially characterised using PIV to estimate a notional induced velocity U_i to scale the descent velocity. The mean axial u and vertical v velocity components extracted on a plane $0.48R$ from the rotor disc plane are shown in Fig. 4.

Based on the time-averaged axial velocity profile of the isolated rotor $u(y)$, the notional induced velocity U_i was calculated to be 3.92 m/s using equation 1 where A_D is the rotor disc area, i.e. πR^2.

$$U_i = \frac{\int_0^R 2\pi u(y) y dy}{A_D} \tag{1}$$

At low rotor separations S, interference effects between the rotors may influence their performance, therefore the notional induced velocity of the isolated rotor U_i was used to scale the descent velocity U_o of both the quadcopter and tandem rotor configurations $\alpha = |U_o|/U_i$.

3.1.2. Multi Rotor

The mean flow fields produced by the quadcopter and tandem rotors, operating in hover as the ro-

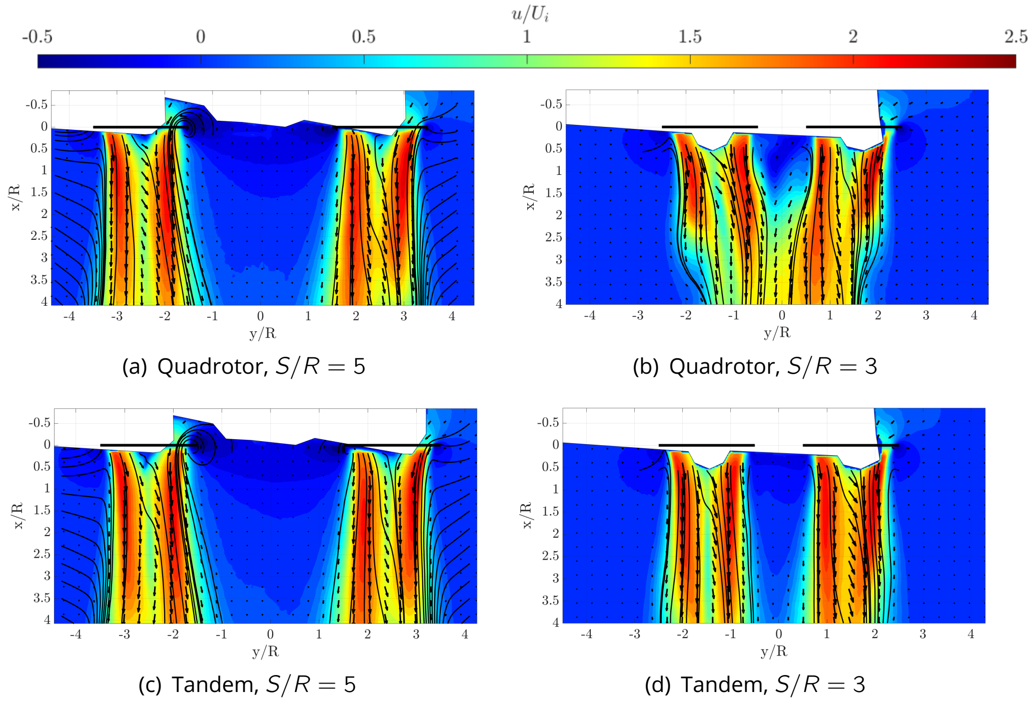

(a) Quadrotor, $S/R = 5$ (b) Quadrotor, $S/R = 3$

(c) Tandem, $S/R = 5$ (d) Tandem, $S/R = 3$

Figure 5: Contour plots of the averaged axial u velocity of the quadcopter (top) and tandem rotors (bottom) operating in hover ($\alpha = 0$), for two rotor separation distances. Velocity is scaled with respect to the notional induced velocity U_i produced by the isolated rotor.

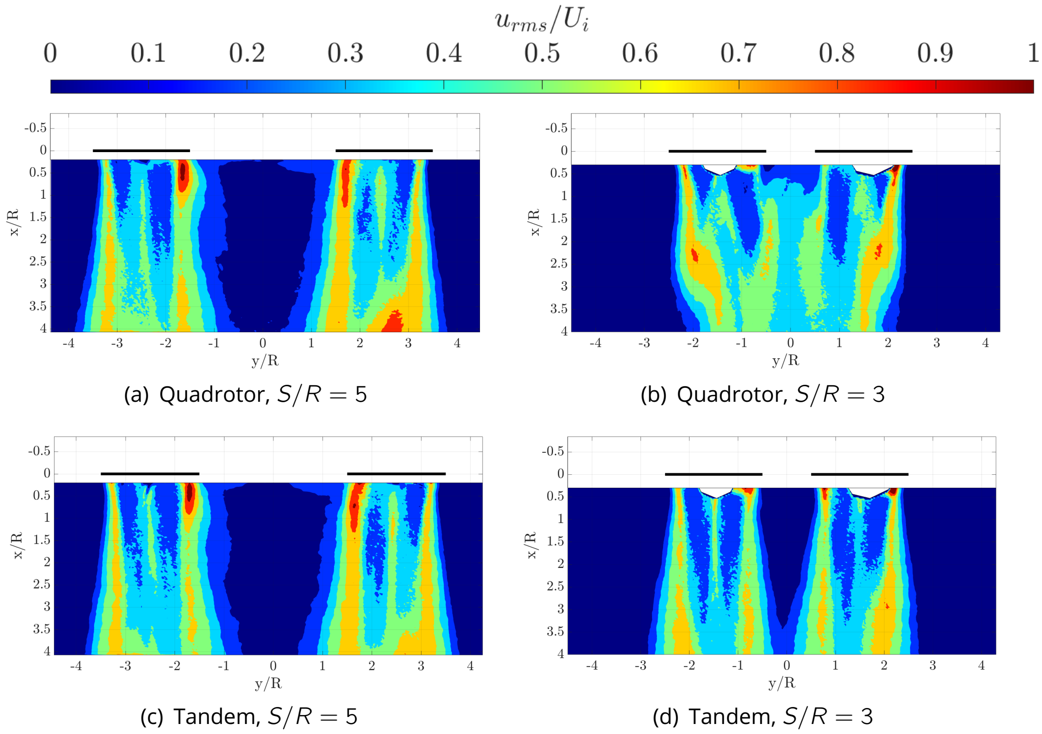

(a) Quadrotor, $S/R = 5$ (b) Quadrotor, $S/R = 3$

(c) Tandem, $S/R = 5$ (d) Tandem, $S/R = 3$

Figure 6: Contour plots of the RMS of the fluctuations of the axial velocity component produced by the quadcopters and tandem rotor configurations operating in hover ($\alpha = 0$). The thick black line represents the rotor disk planes.

tor displacement S was varied from $S = 5R$ to $3R$ are shown in Fig. 5. At rotor displacements greater than $S/R \geq 5$ the wake from each rotor resembles that of an isolated rotor operating in hover, for both the quadcopter and tandem configurations. However, for the quadcopter case at lower rotor separations, the rotors start to interact with one another deflecting their wakes towards the centre of the quadcopter, until they coalesce in a single wake (diameter of approximately 3R) starting at $S/R = 3$, as shown in Fig. 5(b). This is not observed in the tandem rotor case (Fig. 5(d)), highlighting the importance of the two out-of-plane rotors in the development of the wake coalescence. Previous investigations, Ref. [14] and Ref. [15], show that wake coalescence in tandem rotors can appear but at much smaller separation distances.

Contour plots of the RMS of the fluctuations of the axial velocity component u_{rms} produced by both the quadcopter and tandem rotor configurations are shown in Figure 6 to characterise the flow unsteadiness. It is clear that for larger rotor separations the wake unsteadiness presents itself similarly to the one of an isolated rotor. In this case, the propagation and breakdown of the blade tip vortices along the wake shear layer leads to the formation of two regions of unsteadiness per rotor. which extend and expand as the distance from the rotor disc planes increases.

Conversely, when the rotor wakes coalesce for $S/R = 3$, Fig.6(b), a single large region of unsteadiness can be appreciated at a distance greater than 3 radia from the quadrotor disc plane. As the two inner shear layers merge together, their unsteadiness decreases creating a structure similar to the inner shear layer of a single rotor.

3.2. Flow Field Characterisation In Axial Descent

Figure 7 shows the structure of the mean flow field produced by the quadcopter at two rotor separations, $S/R = 5$ and $S/R = 3$, as the descent velocity ratio was varied from $\alpha = 0.6$ to 1.0. All of the flow fields presented were approximately symmetric about $y = 0$. Therefore, for the sake of compactness, data is shown for a reduced ROI corresponding to approximately half of the flow field $(y \geq -0.75)$.

At a rotor separation of $S/R = 5$, as the descent velocity is increased, the free stream flow penetrates between the rotors and a region of recirculation forms on both sides of the rotor. The rotors appear to undergo separate, independent Vortex Ring States, with a stagnation point appearing upstream of each rotor. Even if the rotors undergo separate VRSs, it is apparent that the mutual interference produce a shift of the stagnation points towards the centre of the quadcopter, so that they are no longer aligned with the centre-line of each individual rotor. To contextualise this observation, the stagnation point of an isolated rotor in the VRS typically occurs on the centre-line of the rotor.

When the rotor separation is reduced to $S/R = 3$ the wakes coalesce, as seen in the hovering case, and the quadcopter undergoes one single, global VRS with the formation of a single stagnation point in line with the centre of the quadcopter. This stagnation point travels closer to the quadcopter as α is increased. In addition, the stagnation point and centre of the wake recirculation appears to always be further away from the rotor than in the $S/R = 5$ case for every α investigated, suggesting that the proximity of the rotors potentially delays the VRS onset.

Figure 8 shows the RMS of the fluctuations of the u velocity component in the same test configurations of Fig.7. A region of large RMS values can be always found in correspondence to the position of the stagnation point, suggesting movement of the stagnation point as the rotor wake penetrates the free stream flow is the main mechanism that contributes to unsteadiness in the flow. For the $S/R = 3$ case this region of high unsteadiness appears to be more spread out and less intense than for $S/R = 5$, suggesting that the wake coalescence might not only delay the onset of VRS but also reduce its intensity in terms of flow oscillations. It can also be noted, especially for the large α cases, that a region of high unsteadiness starts to develop on the side of the rotor ($x/R = 0$) in correspondence to the full VRS onset, which is characterised by the re-ingestion of the tip vortices in the rotor wake.

Figure 9 presents the VRS evolution for varying α for both the quadcopter and tandem configuration in the case of the smaller rotor separation, $S/R = 3$. As already commented for Figure 7, the quadcopter, at this rotor spacing, undergoes a global VRS with the formation of a single stagnation point that moves towards the quadcopter centre as α is increased up to the full formation of the VRS at $\alpha = 1.2$. Conversely the tandem rotors undergo individual VRSs, similarly to what happens to the quadrotor for larger rotor spacing. This again highlights the importance of the two out-of-plane motors in the development of the wake coalescence, which makes the quadrotor undergo a global VRS instead of four separate ones. For the tandem case, the stagnation points are closer to the quadrotor centre than the quadrotor case, again suggesting that the wake coalescence might cause a delay in the VRS onset.

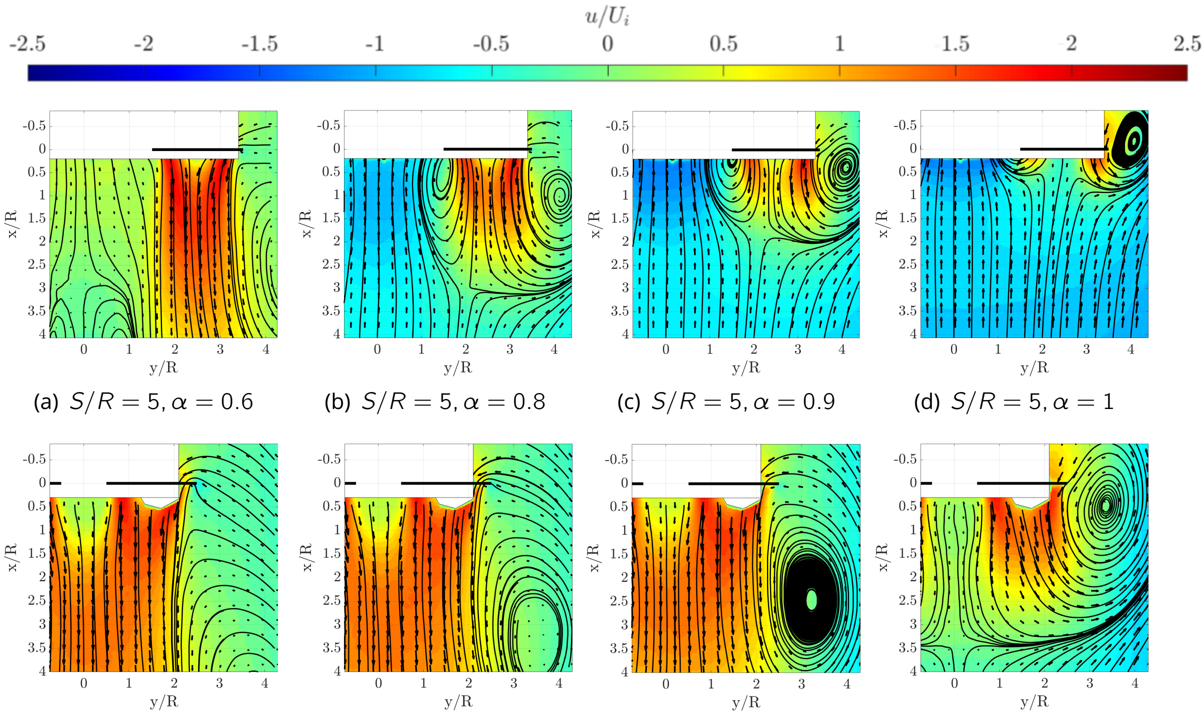

(a) $S/R = 5, \alpha = 0.6$ (b) $S/R = 5, \alpha = 0.8$ (c) $S/R = 5, \alpha = 0.9$ (d) $S/R = 5, \alpha = 1$

(e) $S/R = 3, \alpha = 0.6$ (f) $S/R = 3, \alpha = 0.8$ (g) $S/R = 3, \alpha = 0.9$ (h) $S/R = 3, \alpha = 1$

Figure 7: Contour plots of the averaged axial u velocity and streamlines of the quadcopter with rotor separation $S/R = 5$ (top) and $S/R = 3$ (bottom) for increasing descent velocity ratios α. Velocity is scaled with respect to the notional induced velocity U_i produced by the isolated rotor.

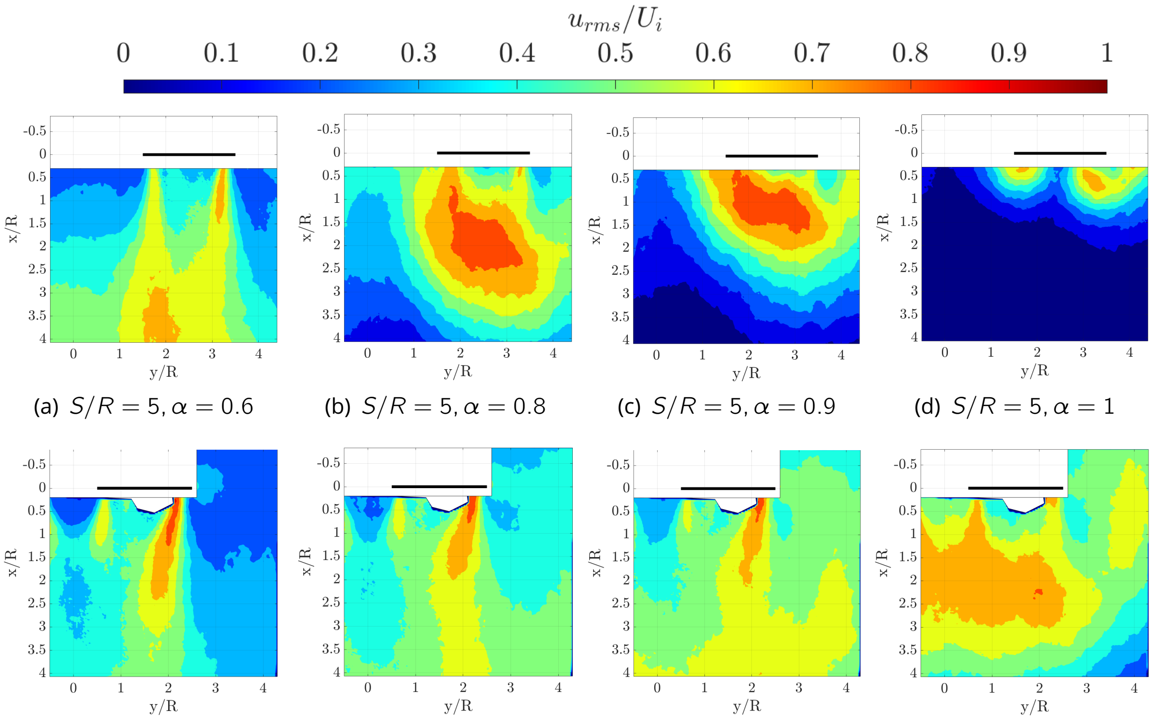

(a) $S/R = 5, \alpha = 0.6$ (b) $S/R = 5, \alpha = 0.8$ (c) $S/R = 5, \alpha = 0.9$ (d) $S/R = 5, \alpha = 1$

(e) $S/R = 3, \alpha = 0.6$ (f) $S/R = 3, \alpha = 0.8$ (g) $S/R = 3, \alpha = 0.9$ (h) $S/R = 3, \alpha = 1$

Figure 8: RMS of the fluctuations of the axial velocity component of the flow field produced by the quadcopter, with a separation distance of $S/R = 5$ (top) and 3 (bottom) as the descent velocity ratio increases from $\alpha - 0.6$ to 1.0. The RMS of the fluctuations is scaled with respect to the notional induced velocity U_i.

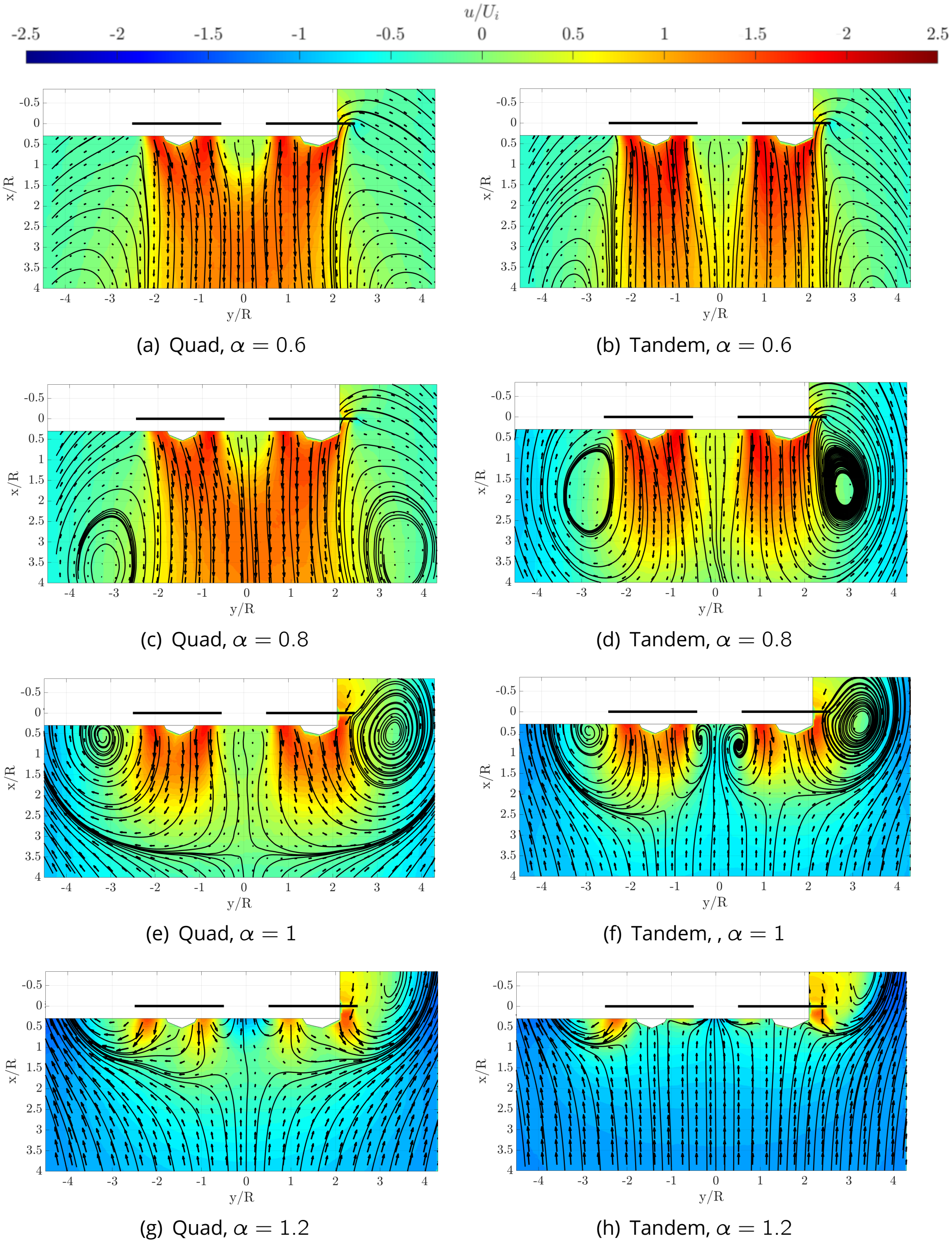

(a) Quad, $\alpha = 0.6$

(b) Tandem, $\alpha = 0.6$

(c) Quad, $\alpha = 0.8$

(d) Tandem, $\alpha = 0.8$

(e) Quad, $\alpha = 1$

(f) Tandem, , $\alpha = 1$

(g) Quad, $\alpha = 1.2$

(h) Tandem, $\alpha = 1.2$

Figure 9: Mean axial velocity contours and streamlines produced by the quadcopter (left) and tandem rotors (right) with a rotor separation of $S/R = 3$, as the descent velocity ratio varies from $\alpha = 0.6$ to $\alpha = 1.2$).

4. CONCLUSIONS

A wind tunnel investigation into flow structure and development of the vortex ring state of multi-rotor configurations was presented. Descent ratios ranged between $\alpha = 0$ to 2 were tested to assess the VRS onset, with counterflow provided from the Handley Page low-speed wind tunnel. Measurements of the flow field were obtained using 2D planar PIV for a custom quadcopter test rig, which allowed testing of both quadcopter and tandem rotor configurations at varying rotor spacings ranging from $S/R = 3$ to 6. Representations of the flow fields were displayed in terms of mean flow and the RMS to highlight variations in the flow unsteadiness. After an hovering analysis of an isolated rotor to compute the reference induced velocity to scale the wind tunnel velocity with, it was shown that:

1. For a hovering quadcopter with rotor separations of 3 radia or less, the rotor wakes coalesce in a single rotor wake with a diameter of 3 radia. the tandem rotor would require much smaller spacings to achieve this.

2. When wake coalescence occurs, the quadrotor undergoes one single global VRS instead of four separate ones.

3. Wake coalescence appears to delay VRS onset and to reduce the unsteadiness of the flow field.

REFERENCES

[1] G. De Bothezat. The general theory of blade screws. *NACA report no.29*, 1919.

[2] J. E. Yeates. Flight measurements of the vibration experienced by a tandem helicopter in transition, vortex-ring state, landing approach and yawed flight. *NACA TN No. 4409*, 1958.

[3] K. Washizu, A. Azuma, J. Koo, and T. Oka. Experimental study on the unsteady aerodynamics of a tandem rotor operating in the vortex ring state. *American Helicopter Society, 22nd Annual Forum, Maryland*, 1966.

[4] M. D. Betzina. Tiltrotor descent aerodynamics: A small-scale experimental investigation of vortex ring state. *American Helicopter Society, 57th Annual Forum, Washington DC.*, 2001.

[5] A. Abrego, M. D. Betzina, and K. R. Long. A small-scale tiltrotor model operating in descending flight. *In 28th European Rotorcraft Forum, Bristol, England.*, 2002.

[6] J. M. Drees and W. P. Hendal. Airflow patterns in the neighbourhood of helicopter rotors. *J. Aircraft Engineering.*, 23(266):107–111, 1951.

[7] J. P. Reeder and F. B. Gustafson. On the flying qualities of helicopters. *NACA-TN-D-1799.*, 1949.

[8] P. Brotherhood. Flow through a helicopter rotor in vertical descent. *Aeronautical Research Committee, R&M No.2735*, 1949.

[9] J. R. Dailey, N. R. Augustine, J. B. Davis, and E. E. Covert. Report of the panel to review the v-22 program. *Technical report, Memorandum for the secretary of defence*, page 14, 2001.

[10] A. Brand, R. Kisor, R. Blyth, D. Mason, and C. Host. V-22 high rate of descent (hrod) test procedures and long record analysis. *American Helicopter Society, 60th Annual Forum, Maryland*, 2004.

[11] S. Chae, S. Lee, and J. Kim. Effects of rotor–rotor interaction on the wake characteristics of twin rotors in axial descent. *Journal of Fluid Mechanics*, 952:A31–1 to A31–27, 2022.

[12] R.E. Brown. Are evtol aircraft inherently more susceptible to the vortex ring state than conventional helicopters? In *48th European Rotorcraft Forum, Winterthur,Switzerland*, 06-08 Sep 2022.

[13] M. Raffel, C. Willert, S. Wereley, and J. Kompenhans. *Particle Image Velocimetry, A Practical Guide. Second Edition*. Springer, 2007.

[14] Seokbong Chae, Seungcheol Lee, and Jooha Kim. Effects of rotor–rotor interaction on the wake characteristics of twin rotors in axial descent. *Journal of Fluid Mechanics*, 952:A31, 2022.

[15] Marcel Veismann, Christopher Dougherty, and Morteza Gharib. Effects of rotor separation on the axial descent performance of dual-rotor configurations. *Flow*, 3:E7, 2023.